MODEL-BASED ROBUST CONTROL OF RESISTIVE WALL MODES VIA μ SYNTHESIS

JOSEPH DALESSIO and EUGENIO SCHUSTER* *Lehigh University*
Mechanical Engineering and Mechanics, Packard Laboratory, Room 550D, Bethlehem, Pennsylvania 18015-3085

DAVID HUMPHREYS and MICHAEL WALKER *General Atomics*
3550 General Atomics Court, San Diego, California 92121

YONGKYOON IN and JIN-SOO KIM *FAR-TECH, Inc.*
3550 General Atomics Court, Building 15, Suite 155, San Diego, California 92121

Received January 17, 2008
Accepted for Publication October 8, 2008

In this work, μ synthesis is employed to stabilize a model of the resistive wall mode (RWM) instability in the DIII-D tokamak. The General Atomics/FAR-TECH DIII-D RWM model, which replaces the spatial perturbation of the plasma with an equivalent perturbation of surface current on a spatially fixed plasma boundary, is used to derive a linear state-space representation of the mode dynamics. The spatial and current perturbations are equivalent in the sense that they both produce the same magnetic field perturbation at surrounding conductors. The key term in the model characterizing the magnitude of the instability is the time-varying uncertain parameter c_{pp}, which is related to the RWM growth rate γ. Taking advantage of the structure of the state matrices, the model is reformulated into a robust control framework, with the growth rate of the RWM modeled as an uncertain parameter. A robust controller that stabilizes the system for a range of practical growth rates is proposed. The controller is tested through simulations, demonstrating significant performance increase over the classical proportional-derivative controller, extending the RWM growth rate range for which the system is stable and satisfies predefined performance constraints, and increasing the level of tolerable measurement noise. The simulation study shows that the proposed model-based DK controllers can successfully stabilize the mode when the growth rate varies over time during the discharge because of changes in the operating conditions such as pressure and rotation. In terms of robust stability, this method eliminates the need for growth-rate online identification and controller scheduling.

KEYWORDS: *RWM stabilization, model-based robust control, structured singular value control synthesis*

Note: Some figures in this paper are in color only in the electronic version.

I. INTRODUCTION

One of the major nonaxisymmetric instabilities in tokamaks is the resistive wall mode (RWM), a form of plasma kink instability whose growth rate is moderated by the influence of a resistive wall.[1] This instability is present in sufficiently high-pressure plasmas in which the plasma kinks in a similar manner to that of a garden hose. In a kink mode, the entire plasma configuration deforms in a helically symmetric manner with an extremely fast growth time (a few microseconds) generating time-varying magnetic perturbations that induce eddy currents in the surrounding conductive structure. These induced currents, in turn, generate magnetic fields that oppose the plasma deformation, slowing the overall growth rate of the instability (to a few milliseconds), which allows the use of feedback to control the RWM. If the surrounding structure were perfectly conductive at a critical distance from the plasma, the system would be stabilized by the mode-induced eddy currents; however, the resistive losses cause a decay in the wall currents, which allow for growth in the mode amplitude. Recent numerical and analytical efforts on modeling the coupling between the plasma and the resistive wall include Refs. 2

*E-mail: schuster@lehigh.edu

through 6. At present, research efforts focus on the stabilization of the $n = 1$ RWM (the plasma perturbation repeats only once as the toroidal angle varies from 0 to 2π) because this instability is usually the first to occur when pressure increases.

The General Atomics (GA)/FAR-TECH DIII-D RWM model represents the perturbed magnetic field on the plasma surface as a toroidal current sheet and represents the resistive wall using an eigenmode approach.[7,8] The plasma surface and current sheet perturbations are equivalent in the sense that they both produce the same magnetic field perturbation at surrounding conductors. Observations from experiments show that the mode spatial structure remains unchanged over a wide range of growth rate.[9] This spatial invariance is described as mode rigidity, which implies that the spatial distribution of current on the plasma surface and the wall remain intact, while only their magnitudes and toroidal phases can change. At extremely high beta, near the ideal stability limit, mode rigidity may not be valid.[10] However, this study assumes mode rigidity as the mode grows as it deals with regimes near the no-wall limit, far away from the ideal-wall limit.

By using a surface-current representation of the mode, it is possible to construct a state-space model of the plant whose states consist only of the surrounding wall current and the external control coil currents. The plasma is represented by the sine and cosine phase components of a "single" mode, which results in many stable system eigenvalues and two unstable system eigenvalues associated with the phase components of the plasma mode. The state-space model, expressed as a set of inductive circuit equations derived from Faraday's Law, is parameterized with a diagonal coupling coefficient matrix C_{pp}, whose entries are directly related to the growth rates of the plasma-mode sine and cosine components. Although in principle the C_{pp} matrix can have different values on its diagonal (reflecting different coupling of the sine and cosine plasma-mode components with nonaxisymmetric conductors), in this study the coupling of the two components of the plasma mode with the conductors is assumed to be identical, and the diagonal values of the C_{pp} matrix are the same. Therefore, the state-space model is finally parameterized by a single scalar value c_{pp}. The two unstable eigenvalues can be viewed as a single eigenvalue of degeneracy two.

Although the plasma surface deformation cannot be directly measured in real time, the magnitude and phase of the deformation can be diagnosed from measurements by a set of 22 magnetic field sensors composed of poloidal probes and saddle loops. A set of 12 internal feedback control coils (I-coils) can then be used to return the plasma to its original axisymmetric shape. Figure 1 shows the arrangement of coils and sensors. Using an estimator for the two orthogonal components of the assumed $n = 1$ mode pattern, the resultant plant can be constructed into a reduced form from the original 12-input, 22-output

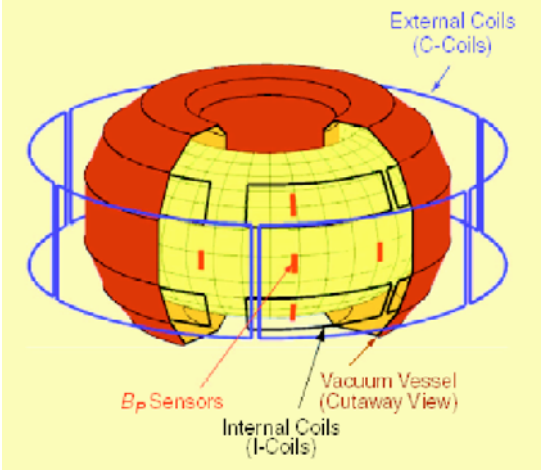

Fig. 1. Coils and sensors for RWM magnetic feedback stabilization.

plant.[11] In particular, using a typical quartet configuration for the I-coils and matched filter, the plant can be simplified to a three-input, two-output system. The quartet configuration reduces the number of controllable inputs by locking the phase of the I-coils in sets of four, 120 deg apart. Thus, the three inputs represent three I-coils that are independently controllable by the quartet configurations. The matched filter reduces the number of observable outputs using a calculated sensor basis vector. For the $n = 1$ mode, the matched filter reduces the 22 outputs to two outputs that represent the RWM vector of the sine and cosine components. These two outputs can be combined to express the output as a signal composed of the RWM amplitude (L^2-norm of the RWM vector) and toroidal phase.[11]

In the past there have been many efforts on feedback stabilization of RWMs in DIII-D (Refs. 12 through 15) as well as in other tokamaks such as HBT-EP (Ref. 16), NSTX (Ref. 17), and ITER, and in reversed field pinch devices such as EXTRAP T2R (Refs. 18 through 21) and RFX-mod (Refs. 22, 23, and 24). Most of the stabilizing efforts in this field focused on designing empirically tuned (non-model-based) controllers with proportional-derivative (PD) action. However, there have been some efforts on developing optimal controllers based on state-space representations of circuit models for a particular growth rate γ of the system [DIII-D (Refs. 25 and 26), ITER (Ref. 27)]. Some of these controllers have been proved effective in extending the stability region of the closed-loop system in simulation studies.

The overall goal of this work is to take advantage of the developed model of the DIII-D RWM system to design a model-based feedback controller for stabilization of the RWM, not for a particular value of the growth rate γ but for a predefined range. The major parameter

characterizing the magnitude of the instability is the time-varying uncertain parameter c_{pp}, which is related through the RWM growth rate γ. This parameter, in the form of the scalar coupling coefficient c_{pp}, is buried within the state-space representation of the plasma and must be extracted and separated from the nominal plant model in order to write the model in a robust control framework. Once the uncertain parameter is extracted, a robust controller, as measured by the structured singular value μ (Ref. 28), is designed to stabilize the RWM instability over a certain range of the growth rate γ. This has the benefit of designing one constant controller that can stabilize the plasma RWM instability over the entire physical range of the uncertain time-varying growth rate.

The paper is organized as follows. Section II introduces the GA/FAR-TECH DIII-D RWM plasma model and manipulates the state-space equation to achieve an affine parameterized form. Section III fully separates the uncertain parameter c_{pp} from the nominal plant using linear fractional transformations (LFTs). Section IV describes the design of a robust controller based on the parameterized model using the *DK* iteration for μ synthesis; the performance of this controller is also assessed through simulations. Section V closes the paper stating the conclusions.

II. PLASMA MODEL AND PARAMETERIZATION

II.A. System Model

Stated below is the GA/FAR-TECH DIII-D RWM model, a plasma response model for the RWM using a toroidal current sheet to represent the plasma surface[7] where no plasma rotation is assumed. Most of the matrices and variables presented are characteristics of the tokamak and are well known. The state-space model is parameterized with a diagonal coupling coefficient matrix C_{pp}, which can be regarded as a reluctance matrix.[29] In this study the coupling of the two phase components of the plasma mode with the conductors is assumed to be identical, and it is possible to write $C_{pp} = c_{pp}I$, where I denotes the 2×2 identity matrix. The model uncertainty is introduced through the single scalar value c_{pp}, which is related to the single unstable mode growth rate γ of the RWM. The relationship between these variables is shown empirically in Fig. 2 for a particular plasma equilibrium and is further explained in Ref. 8.

The model is represented in terms of the couplings between the plasma p, vessel wall w, and coils c. The model derived from Faraday's law of induction results in the system dynamics that reduce to

$$(M_{ss} + M_{sp} C_{pp} M_{ps})\dot{I}_s + R_{ss} I_s = V_s \ ,$$

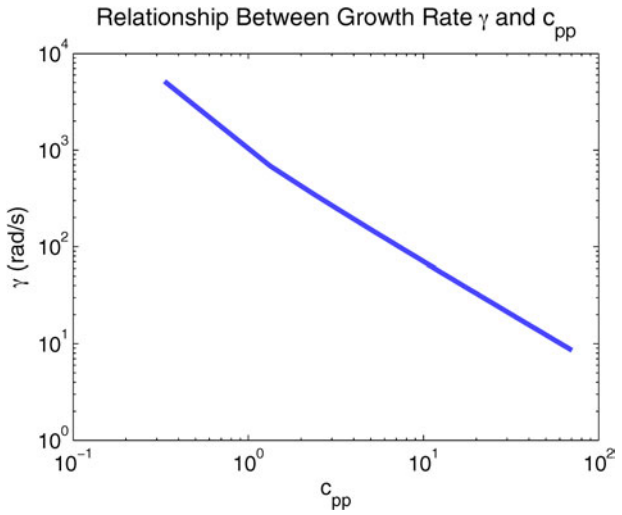

Fig. 2. Empirical relationship between the growth rate γ and c_{pp}.

where

M_{ss} = mutual inductance between external conductors, including the vessel wall and the coils

M_{sp} = mutual inductance between the external conductors and the plasma

R_{ss} = resistance matrix

I_s = current flowing in the conductors

V_s = externally applied voltage to the conductors.

The matrix dimensions depend on the number of eigenmodes used for the model (two states are associated with each eigenmode) and the coil configuration that determines the number of inputs. The mutual inductance matrices are given by

$$M_{ss} = \begin{bmatrix} M_{ww} & M_{wc} \\ M_{cw} & M_{cc} \end{bmatrix} \ , \quad M_{sp} = \begin{bmatrix} M_{wp} \\ M_{cp} \end{bmatrix} \ ,$$

$$M_{ps} = [M_{pw} \quad M_{pc}] \ ,$$

where M_{ps} and M_{sp} satisfy the following condition:

$$M_{ps} = M_{sp}^T = [M_{wp}^T \quad M_{cp}^T] \Rightarrow M_{pw} = M_{wp}^T \ , \quad M_{pc} = M_{cp}^T \ .$$

The resistance matrix is given by

$$R_{ss} = \begin{bmatrix} \lambda_w & 0 \\ 0 & R_c \end{bmatrix} \ ,$$

where λ_w characterizes the mutual resistance matrix of the various eigenmodes of the wall and R_c is the coil resistance matrix. The current and externally applied voltage to the conductors can be written as

$$I_s = \begin{bmatrix} I_w \\ I_c \end{bmatrix} , \quad V_s = \begin{bmatrix} 0 \\ V_c \end{bmatrix} ,$$

where

I_w = wall current

I_c = coil current

V_c = externally applied voltage to the coil.

This model can be represented in a state-space formulation using the current in the conductors as the states ($x = I_s$) and the applied voltage as the inputs ($u = V_s$). This results in the following state-space equation:

$$\dot{x} = Ax + Bu ,$$

where

$$A = -L_{ss}^{-1} R_{ss} , \quad B = L_{ss}^{-1} , \tag{1}$$

and $L_{ss} = M_{ss} - M_{sp} C_{pp} M_{ps}$. The output equation of the state-space representation is based on sensor measurements that relate to the conductor currents through the dynamics

$$y = (C_{ss} - C_{yp} C_{pp} M_{ps}) I_s ,$$

where C_{yp} is the coupling matrix between the sensor and plasma current and

$$C_{ss} = [C_{yw} \quad C_{yc}]$$

is given by the coupling matrix between the sensor and wall current C_{yw}, and the coupling matrix between the sensor and coil current C_{yc}. This results in the state-space output equation

$$y = Cx ,$$

where

$$C = C_{ss} - C_{yp} C_{pp} M_{ps} .$$

II.B. Parameterization of the L_{ss}^{-1} Matrix

The goal of this section is to extract the uncertain parameter c_{pp} from the uncertain state-space system and introduce it as an uncertainty block that perturbs a nominal state-space system. The initial step to obtaining the nominal state-space system is to express each state matrix as a general affine state-space representation using nonlinear functions of the uncertainty c_{pp}. As seen in Eq. (1), the majority of the complexity is introduced in the A and B state matrices, where the uncertainty c_{pp} is introduced through L_{ss}^{-1}, and where $L_{ss} = (M_{ss} - M_{sp} c_{pp} M_{ps})$. Since the instability is two-dimensional (sine and cosine components of the plasma mode), the matrix product $M_{sp} M_{ps}$ is rank 2. Recalling that the 2×2 diagonal C_{pp} matrix is equal to $c_{pp} I$, where I denotes the 2×2 identity matrix, the L_{ss} matrix can be expressed as

$$\begin{aligned} L_{ss} &= M_{ss} - M_{sp} c_{pp} M_{ps} \\ &= M_{ss} - c_{pp} M_{sp} M_{ps} \\ &= M_{ss} - c_{pp} \sum_{i=1}^{2} u_i u_i' , \end{aligned} \tag{2}$$

where

$$M_{sp} = [u_1 \quad u_2] , \quad M_{ps} = \begin{bmatrix} u_1' \\ u_2' \end{bmatrix} ,$$

and

u_1, u_2 = $n \times 1$ vectors

u_1', u_2' = transpose of u_1 and u_2, respectively = $1 \times n$ vectors

n = number of states in the RWM state-space model.

To obtain a parameterized expression for the L_{ss}^{-1} term, we must first compute the inverse of a matrix sum. Given the matrix A_T, the scalar b_T, and the vectors C_T and D_T, the inverse of a matrix sum is given by the Sherman-Morrison formula as[30]

$$(A_T - b_T C_T D_T)^{-1} = A_T^{-1} + \frac{b_T (A_T^{-1} C_T)(D_T A_T^{-1})}{1 - b_T D_T A_T^{-1} C_T} . \tag{3}$$

Using Eq. (2), the inverse of L_{ss} can be written as

$$\begin{aligned} L_{ss}^{-1} &= (M_{ss} - M_{sp} c_{pp} M_{ps})^{-1} \\ &= (M_{ss} - c_{pp} u_1 u_1' - c_{pp} u_2 u_2')^{-1} . \end{aligned}$$

Now, using the matrix $A_l = M_{ss} - c_{pp} u_1 u_1'$, the preceding equation can be written as

$$L_{ss}^{-1} = (A_l - c_{pp} u_2 u_2')^{-1} .$$

This is now in the form given by Eq. (3), and thus, the formula can be applied, resulting in

$$L_{ss}^{-1} = A_l^{-1} + \frac{c_{pp} (A_l^{-1} u_2)(u_2' A_l^{-1})}{1 - c_{pp} u_2' A_l^{-1} u_2} . \tag{4}$$

Now the matrix L_{ss}^{-1} is expressed in terms of A_l^{-1}, which is equivalent to $(M_{ss} - c_{pp} u_1 u_1')^{-1}$, and once again applying Eq. (3) results in

$$\begin{aligned} A_l^{-1} &= (M_{ss} - c_{pp} u_1 u_1')^{-1} \\ &= M_{ss}^{-1} + \frac{c_{pp} (M_{ss}^{-1} u_1)(u_1' M_{ss}^{-1})}{1 - c_{pp} u_1' M_{ss}^{-1} u_1} . \end{aligned}$$

This expression can now be substituted back into Eq. (4). The terms can be collected and rewritten in the following form:

$$B = L_{ss}^{-1} = \sum_{i=0}^{4} \alpha_i B_i \ ,$$

where α_i's are nonlinear functions of c_{pp} and B_i's are constant matrices. The individual terms are given by the following:

$$\alpha_0 = 1$$

$$\alpha_1 = \frac{c_{pp}}{1 - c_{pp} u_1' M_{ss}^{-1} u_1}$$

$$\alpha_2 = \frac{c_{pp}}{1 - c_{pp} u_2' M_{ss}^{-1} u_2 - \dfrac{c_{pp}^2}{1 - c_{pp} u_1' M_{ss}^{-1} u_1} u_2'(M_{ss}^{-1} u_1)(u_1' M_{ss}^{-1}) u_2}$$

$$\alpha_3 = \alpha_2 \alpha_1$$

$$\alpha_4 = \alpha_2 \alpha_1^2$$

$$B_0 = M_{ss}^{-1}$$

$$B_1 = [(M_{ss}^{-1} u_1)(u_1' M_{ss}^{-1})]$$

$$B_2 = [(M_{ss}^{-1} u_2)(u_2' M_{ss}^{-1})]$$

$$B_3 = [(M_{ss}^{-1} u_2)(u_2'(M_{ss}^{-1} u_1)(u_1' M_{ss}^{-1})) + ((M_{ss}^{-1} u_1)(u_1' M_{ss}^{-1}) u_2)(u_2' M_{ss}^{-1})]$$

$$B_4 = [(M_{ss}^{-1} u_1)(u_1' M_{ss}^{-1}) u_2 u_2'(M_{ss}^{-1} u_1)(u_1' M_{ss}^{-1})] \ .$$

II.C. Expressing the Parameterized State-Space Matrices

Section II.B allowed us to express the L_{ss}^{-1} matrix in a parameterized form, which allows the parameterization of the state and input matrices A and B, respectively. In a similar way, the output matrix C can also be parameterized. Using the fact that c_{pp} is a scalar, the C matrix can be written as

$$C = C_{ss} - C_{yp} c_{pp} M_{ps} = C_{ss} - c_{pp} C_{yp} M_{ps}$$
$$= C_0 + \alpha_5 C_5 \ ,$$

where

$$C_0 = C_{ss} \ , \quad C_5 = -C_{yp} M_{ps} \ , \quad \alpha_5 = c_{pp} \ .$$

Defining $A_i = -B_i R_{ss}$, we can finally summarize the parameterized expressions for the state matrices A, B, and C in terms of α_i's, given as

$$A = A_0 + \alpha_1 A_1 + \alpha_2 A_2 + \alpha_3 A_3 + \alpha_4 A_4 \ , \qquad (5)$$

$$B = B_0 + \alpha_1 B_1 + \alpha_2 B_2 + \alpha_3 B_3 + \alpha_4 B_4 \ , \qquad (6)$$

and

$$C = C_0 + \alpha_5 C_5 \ . \qquad (7)$$

III. GROWTH RATE PARAMETERIZATION

III.A. Linear Fractional Transformation of the RWM Model

A system with state-space representation A, B, C, D has a transfer function $G(s) = D + C(sI_n - A)^{-1}B$, where n is the number of states (or eigenvalues) in the system and I_n is the convention used to describe an $n \times n$ identity matrix. Defining the matrix

$$M_\alpha = \begin{bmatrix} A & B \\ C & D \end{bmatrix} \ ,$$

we can write the transfer function as the LFT of M_α as[31]

$$G(s) = F_u\left(\begin{bmatrix} A & B \\ C & D \end{bmatrix}, \frac{1}{s} I_n\right) = F_u\left(M_\alpha, \frac{1}{s} I_n\right)$$
$$= M_{\alpha_{22}} + M_{\alpha_{21}} \frac{1}{s} I_n \left(I_n - M_{\alpha_{11}} \frac{1}{s} I_n\right)^{-1} M_{\alpha_{12}}$$
$$= D + C \frac{1}{s} I_n \left(I_n - A \frac{1}{s} I_n\right)^{-1} B$$
$$= D + C(sI_n - A)^{-1} B \ .$$

The graphical representation of $G(s)$ is shown in Fig. 3, with equivalent equations as follows:

$$\begin{bmatrix} z_1 \\ y \end{bmatrix} = \begin{bmatrix} A & B \\ C & D \end{bmatrix} \begin{bmatrix} w_1 \\ u \end{bmatrix} ,$$

$$w_1 = \frac{1}{s} z_1 ,$$

and

$$y = F_u\left(M_\alpha, \frac{1}{s} I_n\right) u = G(s) u .$$

To introduce the uncertainty given by the parameterized state-space system [Eqs. (5), (6), and (7)], the M_α matrix can be written in the form of a general affine state-space uncertainty:

$$M_\alpha = \begin{bmatrix} A_0 + \sum_{i=1}^{k} \alpha_i A_i & B_0 + \sum_{i=1}^{k} \alpha_i B_i \\ C_0 + \sum_{i=1}^{k} \alpha_i C_i & D_0 + \sum_{i=1}^{k} \alpha_i D_i \end{bmatrix} ,$$

where $k = 5$, $A_5 = 0$, $B_5 = 0$, $C_i = 0$ for $i = 1, \ldots, 4$, and $D_i = 0$ for all i.

This uncertainty can be formulated into an LFT by achieving the smallest possible repeated blocks using the method outlined in Ref. 31. To begin this method, matrices J_i's are formed such that

$$J_i = \begin{bmatrix} A_i & B_i \\ C_i & D_i \end{bmatrix} \in \mathbb{R}^{(n+n_y)\times(n+n_u)}$$

for each $i = 1, \ldots, 5$. Then, using singular value decomposition and grouping terms, an expression for J_i can be obtained (note that A^* is denoted as the complex conjugate transpose of the matrix A):

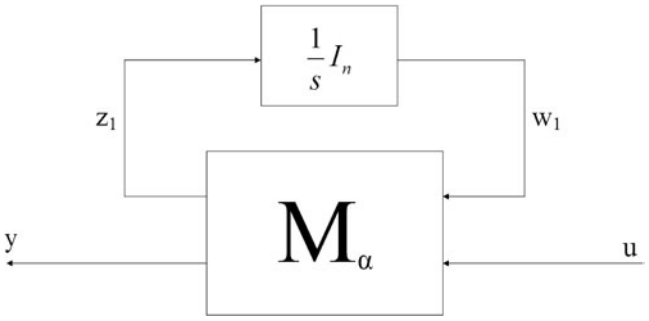

Fig. 3. $G(s)$ as an LFT using M_α, $(1/s)I_n$.

$$J_i = U_i \Sigma_i V_i^* = (U_i \sqrt{\Sigma_i})(\sqrt{\Sigma_i} V_i^*)$$

$$= \begin{bmatrix} L_i \\ W_i \end{bmatrix} \begin{bmatrix} R_i \\ Z_i \end{bmatrix}^* .$$

Denoting q_i as the rank of each matrix J_i, each inner matrix is given by

$$L_i \in \mathbb{R}^{(n\times q_i)} , \quad W_i \in \mathbb{R}^{(n_y\times q_i)} , \quad R_i \in \mathbb{R}^{(n\times q_i)} ,$$

$$Z_i \in \mathbb{R}^{(n_u\times q_i)} .$$

Then, the uncertainty can be introduced as

$$\alpha_i J_i = \begin{bmatrix} L_i \\ W_i \end{bmatrix} [\alpha_i I_{q_i}] \begin{bmatrix} R_i \\ Z_i \end{bmatrix}^* ,$$

where for this particular equilibrium,

$$q_1 = 1 ,$$

$$q_2 = 1 ,$$

$$q_3 = 2 ,$$

$$q_4 = 1 ,$$

and

$$q_5 = 2 .$$

Finally, the linear fractional transformed matrix can be written as

$$M_\alpha = M_{11} + M_{12} \alpha_p M_{21} ,$$

where

$$M_{11} = \begin{bmatrix} A_0 & B_0 \\ C_0 & D_0 \end{bmatrix} , \quad M_{12} = \begin{bmatrix} L_1 & \cdots & L_5 \\ W_1 & \cdots & W_5 \end{bmatrix}$$

$$M_{21} = \begin{bmatrix} R_1^* & Z_1^* \\ \vdots & \vdots \\ R_5^* & Z_5^* \end{bmatrix} , \quad \alpha_p = \begin{bmatrix} \alpha_1 I_{q_1} & & 0 \\ & \ddots & \\ 0 & & \alpha_5 I_{q_5} \end{bmatrix} .$$

This is equivalent to the lower LFT:

$$M_\alpha = F_l\left(\begin{bmatrix} M_{11} & M_{12} \\ M_{21} & 0 \end{bmatrix}, \alpha_p\right) = F_l(M, \alpha_p)$$

$$= M_{11} + M_{12} \alpha_p (I_{q_T} - M_{22} \alpha_p)^{-1} M_{21}$$

$$= M_{11} + M_{12} \alpha_p M_{21} ,$$

where

$$M = \begin{bmatrix} M_{11} & M_{12} \\ M_{21} & 0 \end{bmatrix}$$

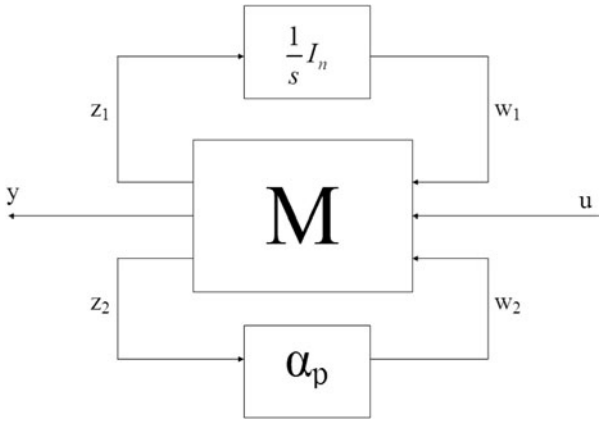

Fig. 4. $G(s)$ as an LFT using M, α_p, $(1/s)I_n$.

and q_T is the total rank of the α_p matrix given by

$$q_T = \sum_i q_i = 7 \ .$$

Finally, the transfer function of the uncertain state-space model is written as

$$G(s) = F_u\left(M_\alpha, \frac{1}{s} I_n\right) = F_u\left(F_l(M, \alpha_p), \frac{1}{s} I_n\right) \ .$$

The graphical representation of $G(s)$ is shown in Fig. 4, with the equivalent equations as follows:

$$\begin{bmatrix} \begin{bmatrix} z_1 \\ y \end{bmatrix} \\ z_2 \end{bmatrix} = \begin{bmatrix} M_{11} & M_{12} \\ M_{21} & 0 \end{bmatrix} \begin{bmatrix} \begin{bmatrix} w_1 \\ u \end{bmatrix} \\ w_2 \end{bmatrix} \ ,$$

$$w_1 = \frac{1}{s} z_1 \ , \quad w_2 = \alpha_p z_2 \ ,$$

and

$$y = F_u\left(F_l(M, \alpha_p), \frac{1}{s} I_n\right) u = G(s) u \ .$$

III.B. Normalizing the α Parameters

The system is now in a form where the uncertainty is given by the five α_i parameters. However, as shown earlier, each of the α_i parameters is a nonlinear function of the single variable c_{pp}. Thus, the next step is to express the LFT in terms of the single uncertainty c_{pp}. First, c_{pp} is normalized using

$$c_{pp} = d + \delta e \ ,$$

$$d = c_{pp}^* \ ,$$

and

$$e = \max[\,|c_{pp_{\max}} - c_{pp}^*|, |c_{pp_{\min}} - c_{pp}^*|\,] \ ,$$

where c_{pp}^* is the nominal value of c_{pp}, and $c_{pp_{\min}}$ and $c_{pp_{\max}}$ are its minimum and maximum values, respectively. This defines a new normalized uncertainty δ that has a range of values within $|\delta| \le 1$ that corresponds to the desired c_{pp} range.

Now that each α_i parameter is expressed in terms of δ, we "pull out the δ" (Ref. 28). This is done by drawing the block diagram for each α_i system and labeling the input to each δ block z_{3_i} and the output of each δ block w_{3_i}. Then the matrix Q, which satisfies $\alpha_p = F_l(Q, \Delta)$ with $\Delta = \delta I_{m_T}$, can be found using

$$\begin{bmatrix} w_{2_i} \\ z_{3_i} \end{bmatrix} \triangleq Q_i \begin{bmatrix} z_{2_i} \\ w_{3_i} \end{bmatrix}$$

for each α_i term, where m_T is the total number of uncertainty elements needed to represent α_p. Thus, the Q_i matrix satisfies the equation $\alpha_i = F_l(Q_i, \delta I_{m_i})$, where m_i is the minimum number of uncertainty elements δ needed to represent α_i. Recalling that $w_2 = \alpha_p z_2$, the system can be formulated such that $w_2 = F_l(Q, \Delta) z_2$. To correspond to each α_i term in the matrix α_p, the w_2, z_2, w_3, z_3 matrices are given by

$$w_2 = \begin{bmatrix} w_{2_1} \\ w_{2_2} \\ w_{2_3} \\ w_{2_4} \\ w_{2_5} \end{bmatrix} \ , \quad z_2 = \begin{bmatrix} z_{2_1} \\ z_{2_2} \\ z_{2_3} \\ z_{2_4} \\ z_{2_5} \end{bmatrix} \ ,$$

$$w_3 = \begin{bmatrix} w_{3_1} \\ w_{3_2} \\ w_{3_3} \\ w_{3_4} \\ w_{3_5} \end{bmatrix} \ , \quad z_3 = \begin{bmatrix} z_{3_1} \\ z_{3_2} \\ z_{3_3} \\ z_{3_4} \\ z_{3_5} \end{bmatrix} \ ,$$

where w_{2_i} and z_{2_i} are vectors of length q_i, based on the rank of each J_i matrix, and w_{3_i} and z_{3_i} are vectors of length $m_i q_i$, based on the minimum number of δ's required to represent each α_i and the value of q_i. The composite Q matrix will be defined after each individual Q_i is determined, where Q_i is given by

$$Q_i = \begin{bmatrix} Q_{i_{11}} & Q_{i_{12}} \\ Q_{i_{21}} & Q_{i_{22}} \end{bmatrix} \ .$$

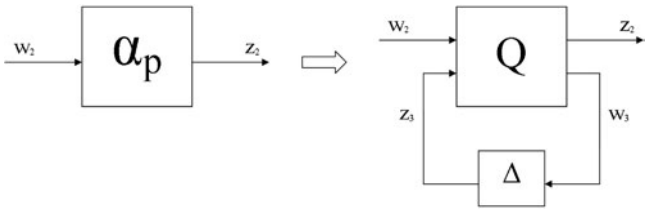

Fig. 5. α_p as an LFT using Q and Δ.

The total number of uncertainty elements m_T for α_p is given by the total length of w_3, which is found by

$$m_T = \sum_i m_i q_i \ .$$

The graphical representation of the α_p block is show in Fig. 5.

The block diagram for α_1 is shown in Fig. 6. Recalling that $\alpha_1 = c_{pp}/(1 - c_{pp} u_1' M_{ss}^{-1} u_1)$, and using $a = u_1' M_{ss}^{-1} u_1$, the relationship becomes

$$\alpha_1 = \frac{c_{pp}}{1 - a c_{pp}} \ .$$

Inserting the normalized relationship $c_{pp} = d + \delta e$, α_1 can be written as

$$\alpha_1 = \frac{d + \delta e}{1 - a(d + \delta e)} = \frac{d + \delta e}{(1 - ad) - ae\delta} \ .$$

Since there is only one uncertainty element, $m_1 = 1$. The block diagram for α_1 can be directly drawn from this form, with the feedback terms in the denominator and the feedforward terms in the numerator. From the diagram,

$$z_{3_1} = z_{2_1} + (a d z_{3_1} + a e w_{3_1}) \ .$$

Solving for z_{3_1},

$$z_{3_1} - ad z_{3_1} = z_{2_1} + ae w_{3_1} \ ,$$

$$z_{3_1}(1 - ad) = z_{2_1} + ae w_{3_1} \ ,$$

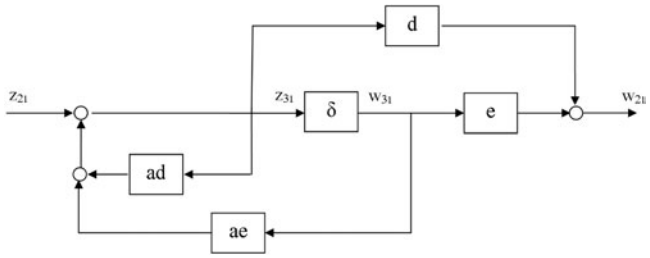

Fig. 6. Block diagram for α_1.

and

$$z_{3_1} = \left(\frac{1}{1 - ad}\right) z_{2_1} + \left(\frac{ae}{1 - ad}\right) w_{3_1} \ .$$

From the diagram, the output is given by

$$w_{2_1} = d z_{3_1} + e w_{3_1} \ .$$

Substituting for z_{3_1}, the expression becomes

$$\begin{aligned} w_{2_1} &= d\left[\left(\frac{1}{1 - ad}\right) z_{2_1} + \left(\frac{ae}{1 - ad}\right) w_{3_1}\right] + e w_{3_1} \\ &= \left(\frac{d}{1 - ad}\right) z_{2_1} + \left(\left[\frac{aed}{1 - ad}\right] + e\right) w_{3_1} \\ &= \left(\frac{d}{1 - ad}\right) z_{2_1} + \left(e\left[1 + \frac{ad}{1 - ad}\right]\right) w_{3_1} \ . \end{aligned}$$

Thus, the governing equation for α_1 is given by

$$\begin{bmatrix} w_{2_1} \\ z_{3_1} \end{bmatrix} = Q_1 \begin{bmatrix} z_{2_1} \\ w_{3_1} \end{bmatrix} \ ,$$

which results in a Q_1 given by

$$Q_1 = \begin{bmatrix} \dfrac{d}{1 - ad} & e\left[1 + \dfrac{ad}{1 - ad}\right] \\ \dfrac{1}{1 - ad} & \dfrac{ae}{1 - ad} \end{bmatrix} = \begin{bmatrix} Q_{1_{11}} & Q_{1_{12}} \\ Q_{1_{21}} & Q_{1_{22}} \end{bmatrix} \ .$$

For the system matrices of the DIII-D tokamak under the particular equilibrium, the behavior of α_1 and α_2 is approximately the same, with an error on the order of 10^{-12}. From this very good approximation, we can take $\alpha_1 = \alpha_2$. Although the full model could be used, this is an accurate enough assumption that allows the reduction of computational complexity. As a result of this approximation, the following changes can be made to the other α parameters:

$$\alpha_3 = \alpha_2 \alpha_1 \Rightarrow \alpha_3 = \alpha_1^2$$

and

$$\alpha_4 = \alpha_2 \alpha_1^2 \Rightarrow \alpha_4 = \alpha_1^3 \ .$$

Since $\alpha_2 = \alpha_1$, $m_2 = m_1 = 1$ and the Q_2 block is simply defined by

$$Q_2 = Q_1 \ .$$

The parameter α_3 is given as $\alpha_3 = \alpha_1^2$, or $\alpha_3 = F_l(Q_1,\delta)\cdot F_l(Q_1,\delta)$. In general, the series connection of l identical lower LFTs $F_l(T,\delta)$, where

$$T = \begin{bmatrix} T_{11} & T_{12} \\ T_{21} & T_{22} \end{bmatrix},$$

can be written as $F_l(S,\delta I_l)$, where

$$S = \left[\begin{array}{c|ccccc} T_{11}^l & T_{11}^{l-1}T_{12} & T_{11}^{l-2}T_{12} & \cdots & T_{11}T_{12} & T_{12} \\ \hline T_{21} & T_{22} & & \cdots & & 0 \\ T_{21}T_{11} & T_{21}T_{12} & T_{22} & & & \\ \vdots & \vdots & T_{21}T_{12} & T_{22} & & \vdots \\ T_{21}T_{11}^{l-2} & T_{21}T_{11}^{l-3}T_{12} & \iddots & T_{21}T_{12} & T_{22} & \\ T_{21}T_{11}^{l-1} & T_{21}T_{11}^{l-2}T_{12} & T_{21}T_{11}^{l-3}T_{12} & \cdots & T_{21}T_{12} & T_{22} \end{array}\right].$$

A reduction can be made so that $\alpha_3 = F_l(Q_3,\delta I_2)$, where I_2 is the size 2 identity matrix, thus $m_3 = 2$. Through the series connection of the LFT of Q_1, the Q_3 block is given by

$$Q_3 = \left[\begin{array}{c|cc} Q_{1_{11}}^2 & Q_{1_{11}}Q_{1_{12}} & Q_{1_{12}} \\ \hline Q_{1_{21}} & Q_{1_{22}} & 0 \\ Q_{1_{21}}Q_{1_{11}} & Q_{1_{21}}Q_{1_{12}} & Q_{1_{22}} \end{array}\right].$$

Similarly to Q_3, the parameter α_4 is given as $\alpha_4 = \alpha_1^3$, or $\alpha_4 = F_l(Q_1,\delta)\cdot F_l(Q_1,\delta)\cdot F_l(Q_1,\delta)$. A reduction can be made so that $\alpha_4 = F_l(Q_4,\delta I_3)$, where I_3 is the size 3 identity matrix, $m_4 = 3$, and Q_4 is given by the series connection of the LFT such that

$$Q_4 = \left[\begin{array}{c|ccc} Q_{1_{11}}^3 & Q_{1_{11}}^2Q_{1_{12}} & Q_{1_{11}}Q_{1_{12}} & Q_{1_{12}} \\ \hline Q_{1_{21}} & Q_{1_{22}} & 0 & 0 \\ Q_{1_{21}}Q_{1_{11}} & Q_{1_{21}}Q_{1_{12}} & Q_{1_{22}} & 0 \\ Q_{1_{21}}Q_{1_{11}}^2 & Q_{1_{21}}Q_{1_{11}}Q_{1_{12}} & Q_{1_{21}}Q_{1_{12}} & Q_{1_{22}} \end{array}\right].$$

Also, Q_5 can be directly written as

$$Q_5 = \begin{bmatrix} d & e \\ 1 & 0 \end{bmatrix},$$

such that $m_5 = 1$.

Now that there is an expression for each of the α_i $(i = 1,\ldots,5)$ parameters in terms of an LFT $\alpha_i = F_l(Q_i,\delta I_{m_i})$, they can be combined to form one LFT with a common uncertainty δ. As shown earlier, the uncertainty in terms of α is given as

$$\alpha_p = \begin{bmatrix} \alpha_1 I_{q_1} & & & & 0 \\ & \alpha_2 I_{q_2} & & & \\ & & \alpha_3 I_{q_3} & & \\ & & & \alpha_4 I_{q_4} & \\ 0 & & & & \alpha_5 I_{q_5} \end{bmatrix},$$

where I_{q_i} is the size q_i identity matrix. The total number of uncertain elements is given by $m_T = \sum_i m_i q_i = 11$. Thus, the linear fractional transformation $\alpha_p = F_l(Q,\Delta)$ with $\Delta = \delta I_{m_T}$ is given by $\alpha_p = Q_{11} + Q_{12}\Delta(I_{m_T} - Q_{22}\Delta)^{-1}Q_{21}$, where

$$Q = \begin{bmatrix} Q_{11} & Q_{12} \\ Q_{21} & Q_{22} \end{bmatrix}.$$

Each submatrix Q_{jk} is given by the block diagonal matrix

$$Q_{jk} = \begin{bmatrix} Q_{1_{jk}} & & 0 \\ & \ddots & \\ 0 & & Q_{5_{jk}} \end{bmatrix},$$

where $j = 1,2$ and $k = 1,2$. The matrix Q_{jk} has the same number of diagonal blocks as α_p based on the rank of each J_i matrix denoted by q_i.

III.C. Model in Robust Control Framework

The final expanded representation of the entire system is $G(s) = F_u(F_l(M,F_l(Q,\Delta)),(1/s)I_n)$, which is described by Fig. 7 and the corresponding equation set:

$$\begin{bmatrix} \begin{bmatrix} z_1 \\ y \end{bmatrix} \\ z_2 \end{bmatrix} = \begin{bmatrix} M_{11} & M_{12} \\ M_{21} & 0 \end{bmatrix} \begin{bmatrix} \begin{bmatrix} w_1 \\ u \end{bmatrix} \\ w_2 \end{bmatrix},$$

$$\begin{bmatrix} w_2 \\ z_3 \end{bmatrix} = \begin{bmatrix} Q_{11} & Q_{12} \\ Q_{21} & Q_{22} \end{bmatrix} \begin{bmatrix} z_2 \\ w_3 \end{bmatrix},$$

$$w_1 = \frac{1}{s} z_1 \ , \quad w_3 = \delta z_3 \ ,$$

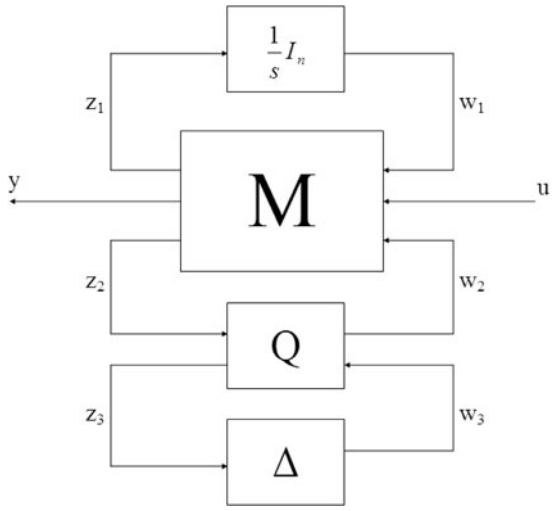

Fig. 7. $G(s)$ as an LFT using M, Q, δ, $(1/s)I_n$.

and

$$y = F_u\left(F_l(M, F_l(Q,\Delta)), \frac{1}{s} I_n\right)u = G(s)u \ .$$

Finally, the original system M can be combined with the matrix Q through the interconnection of LFTs (Ref. 32). This is done using the fact that

$$M_\alpha = F_l(M, \alpha_p) = F_l(M, F_l(Q,\Delta)) = F_l(R,\Delta) \ ,$$

where R is defined as

$$R \triangleq \begin{bmatrix} R_{11} & R_{12} \\ R_{21} & R_{22} \end{bmatrix} ,$$

and where

$$R_{11} = M_{11} + M_{12}Q_{11}(I_1 - M_{22}Q_{11})^{-1}M_{21}$$

$$R_{12} = M_{12}(I_1 - Q_{11}M_{22})^{-1}Q_{12}$$

$$R_{21} = Q_{21}(I_1 - M_{22}Q_{11})^{-1}M_{21}$$

$$R_{22} = Q_{22} + Q_{21}M_{22}(I_1 - Q_{11}M_{22})^{-1}Q_{12} \ .$$

Since $M_{22} = 0$, it simplifies to

$$R = \begin{bmatrix} M_{11} + M_{12}Q_{11}M_{21} & M_{12}Q_{12} \\ Q_{21}M_{21} & Q_{22} \end{bmatrix} .$$

Now the system is reduced to a simple form of R, uncertainty $\Delta = \delta I_{m_T}$ with $|\delta| \le 1$, and $(1/s)I_n$. The system can now be reduced using a simple property of the LFT. The system given by $G(s) = F_u(F_l(R,\Delta),(1/s)I_n)$ can be written as $G(s) = F_l(F_u(R,$

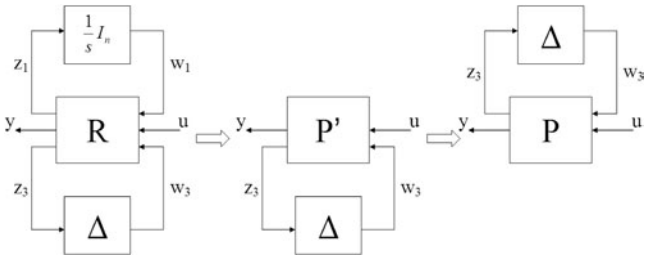

Fig. 8. Graphical representation of $G(s)$ manipulation.

$(1/s)I_n),\Delta) = F_l(P',\Delta)$, where $P' = F_u(R,(1/s)I_n)$. The final step in the system reduction moves the uncertainty, creating an upper LFT for convention purposes. This is done by using

$$G(s) = F_l(P',\Delta) = F_u(P,\Delta) \ ,$$

where P' is of the form

$$P' = \begin{bmatrix} P'_{11} & P'_{12} \\ P'_{21} & P'_{22} \end{bmatrix} \quad \text{and} \quad P = \begin{bmatrix} P'_{22} & P'_{21} \\ P'_{12} & P'_{11} \end{bmatrix} .$$

The overall system reduction is shown in Fig. 8. The parameterization of the RWM model allows this system to be represented in the general framework of robust control for uncertain systems. The goal is to design a controller K that stabilizes the plant for all uncertainty $|\delta| \le 1$. The feedback controller K can be applied to the plant to formulate a closed-loop LFT system on the uncertainty and the controller, given by

$$G(s) = F_l(F_u(P,\Delta),K)$$

$$= F_u(F_l(P,K),\Delta) \ ,$$

which can be seen in Fig. 9.

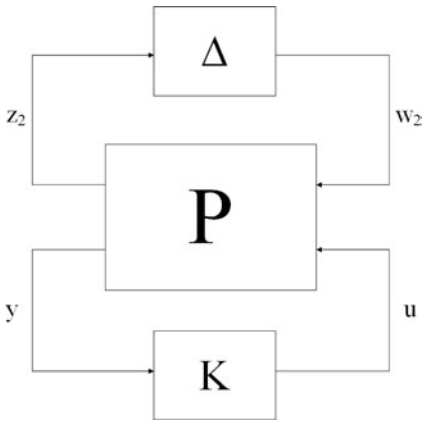

Fig. 9. General framework for robust control.

IV. CONTROLLER SYNTHESIS AND SIMULATION

IV.A. *DK* Iteration Model–Based Controller

Experimentally, the growth rate can vary from very low (or even stable) to very high as higher β_N and/or strong rotation slowing down occurs. Indeed, DIII-D can often transition to a growth rate that is apparently uncontrollable as the rotation crashes to zero. A successful controller must be able to stabilize the system as the growth rate transitions across this entire range in a single discharge (or a gain scheduled sequence of controllers must be rapidly switched in during such transition, which is not expected to be practical). The goal of this work is to design one controller that can robustly stabilize the RWM and meet specified controller performance criteria (Table I). That is equivalent to designing a feedback controller K that robustly stabilizes the system for the applicable range of Δ in Fig. 9. The basic idea is that for a small enough change in the uncertain parameter (growth rate), stability can be maintained. Thus, μ analysis gives a nonconservative measure of the range of change for the uncertain parameter in which the system remains stable and the performance criterion is satisfied. The robust stability of the plant is determined by the N_{11} submatrix, where $N = F_l(P, K)$. The system N represents the nominal closed-loop system. The subsystem N_{11} term isolates the uncertainty from the input and output of the system. Meanwhile, N_{12} and N_{21} characterize the coupling between the uncertainty and the input/output of the system, and N_{22} represents the system at a nominal c_{pp} value ($\Delta = 0$). The robust stability is determined by the structured singular value, which is defined as

$$\mu(N_{11}) \triangleq \frac{1}{\min\{k_m | \det(I - k_m N_{11}\Delta) = 0\}}$$

for $\bar{\sigma}(\Delta) \leq 1$. Larger μ values means $(I - N_{11}\Delta)$ becomes singular with small perturbations, thus the smaller μ the better. The robust stability condition is found by finding the smallest value of k_m at the onset of instability, or $\det(I - k_m N_{11}\Delta) = 0$, which yields $k_m = 1/\mu(N_{11})$, where k_m is a measure of the robust stability to perturbations in Δ. Thus, assuming N_{11} and Δ are stable, the system is robustly stable if and only if $\mu(N_{11}(j\omega)) < 1$, $\forall\omega$. Similarly, the robust performance is given by $\mu(N) < 1$, $\forall\omega$. Both conditions assume that N is internally stable.

TABLE I

Performance Targets and Constraints

Condition	Target Value	Maximum Constraint
Rise time	1.0 ms	5.0 ms
Settling time	5.0 ms	10 ms
Overshoot	15%	50%
Input voltage	N/A[a]	±100 V

[a]N/A = not applicable.

One available procedure to design a controller using μ synthesis is *DK* iteration. Since there is no direct method to synthesize a μ-optimal controller, this method is used by combining $\mathcal{H}_\infty$ synthesis and μ analysis. This method starts with the upper bound on μ in terms of the scaled singular value:

$$\mu(N) \leq \min_{D\in\mathcal{D}} \bar{\sigma}(DND^{-1}) \ ,$$

where $\mathcal{D}$ is the set of matrices D that commute with Δ, i.e., $D\Delta = \Delta D$. Then, the controller that minimizes the peak value over frequency of this upper bound is found, namely,

$$\min_K \left(\min_{D\in\mathcal{D}} \| DN(K)D^{-1} \|_\infty \right) \ .$$

The controller is designed by alternating between the two minimization problems until reasonable performance is achieved. The *DK*-iteration steps are summarized in Ref. 32 as follows:

1. *K* step: Synthesize an $\mathcal{H}_\infty$ controller for the scaled problem, $\min_K \| DN(K)D^{-1} \|_\infty$ with fixed $D(s)$.

2. *D* step: Find $D(j\omega)$ to minimize $\bar{\sigma}(DND^{-1}(j\omega))$ at each frequency with fixed N.

3. Fit the magnitude of each element of $D(j\omega)$ to a stable and minimum-phase transfer function $D(s)$ and go to step 1.

The iteration continues until $\| DN(K)D^{-1} \|_\infty < 1$ or the $\mathcal{H}_\infty$ norm no longer decreases.

Using the derived $P - \Delta$ formulation (Fig. 9), a controller can be designed with the *DK*-iteration method for robust stabilization. For the model being used the growth rate γ ranges from 10 to 5000 rad/s. This results in a range for the uncertain parameter c_{pp} that goes from 71 to 0.3325. This is the range of values for which the system should be stabilized so that the robust controller can be considered a suitable design for DIII-D.

The complete system that is used to design the controller has two additional time delay blocks preceding the plasma model. The time delays physically represent the plasma control system and the power supply. For design purposes, the time delays are linearized using second-order Padé approximations.

Two controllers are synthesized using the *dksyn* command in Matlab, one using the nominal plant and the other an augmented plant with input weight. The performance weight is added to the inputs of the system to achieve desired loop-shaping results. The weight is of the

form $W = (M^{-1/n}s + \omega_b^*)^n/(s + \omega_b^* A^{1/n})^n$, where $M = 10^6$, $\omega_b^* = 10^9$, $A = 1$, and $n = 2$. During the process of synthesizing the controller, it is evident that controllers designed with a smaller, more unstable nominal c_{pp} value produce the widest range of stability for c_{pp}. This is because the normalized uncertainty δ is defined by a linear relationship with c_{pp}, while the unstable eigenvalue of the system is nonlinear with respect to c_{pp}. Using a smaller, more unstable c_{pp} range, the defined linear relationship with δ more accurately represents the system by capturing the dynamics at the more unstable values of c_{pp}. The *DK* controller is synthesized using a $P - \Delta$ system constructed for $c_{pp}^* = 0.34125$ ($\gamma^* = 4890$ rad/s) and guarantees $\mu < 1$ for the range defined by

$$c_{pp_{\min}} = 0.3325$$

and

$$c_{pp_{\max}} = 0.35 \ ,$$

which is equivalent to

$$\gamma_{\max} = 5000 \text{ rad/s}$$

and

$$\gamma_{\min} = 4660 \text{ rad/s} \ .$$

However, these results are conservative, and as will be shown in the next part, the stability and performance ranges for our system are indeed bigger. The conservatism is explained by the fact that the *DK*-iteration implicitly assumes that the uncertain parameter is complex and does not take advantage of the known phase information of the real uncertainty. The real uncertainty can be considered using a modified algorithm, the *DGK* iteration.[33] However, this algorithm greatly increases the numerical complexity. The controllers were designed and simulated using a 15-eigenmode model with 36 states. There are two states to describe each eigenmode, three states for the controlled I-coils in the quartet configuration, and three states for the external coils (C-coils). The designed controllers have orders of 108 and 107 for the plant without weight and with weight, respectively. In both cases, the controller order is reduced to 16 (using the Hankel norm model reduction technique[28,32]) before computing the effective stability and performance ranges.

IV.B. Controller Simulation and Results

In order to be able to compare the proposed model-based *DK* controllers with present non-model-based controllers, a PD controller is designed (integral action is not required for this system). The PD controller is synthesized to maximize the stability range as a function of γ and is of the form

$$K_{ij} = \frac{G_{P_{ij}} + G_{D_{ij}} s}{1 + \tau_{pcs} s} \ ,$$

where

i = number of controlled variables = 3

j = number of outputs = 2

G_P = proportional gain

G_D = derivative gain

τ_{pcs} = time constant, taken to be 4×10^{-4} s.

Each K_{ij} term fills the 3×2 controller matrix K. Beginning with a stabilizing controller with $K_{11} = K_{22}$ and every other term set to zero, the stability range of this controller is obtained. Holding these terms constant and individually checking the maximum stability range for the remaining terms under the optimal condition, the only term that had a more stabilizing effect was the K_{32} term. It has been shown that the stability range can be maximized by a controller with nonzero K_{11}, K_{22}, K_{32} terms and every other term set to zero. Using PD controllers for the terms K_{11}, K_{22}, and K_{32}, all six gains are optimized to obtain the maximum range of stability as a function of γ. The resulting gains are

$$G_{P_{11}} = 3.80 \times 10^4 \ ,$$

$$G_{D_{11}} = 76 \ ,$$

$$G_{P_{22}} = 1.38 \times 10^4 \ ,$$

$$G_{D_{22}} = 40 \ ,$$

$$G_{P_{32}} = 6.62 \times 10^4 \ ,$$

and

$$G_{D_{32}} = 103 \ .$$

The performance of the model-based *DK* controllers is simulated using a Simulink model of the plasma, controller, plasma control system, and power supply and is compared to the results of a well-tuned PD controller. The top level of the Simulink model is presented in Fig. 10. The power supply has a time delay and a saturation block that realizes the physical limit of the applied voltage of ± 100 V. The plasma model consists of a control input and an additional input for the varying c_{pp}. The detail of the plasma model in Simulink (Fig. 11) includes the state-space construction using the α parameters [Eqs. (5), (6), and (7)] and noise subsystems comprised of independent random band-limited white noise generators. Table I provides the performance constraints in response to a unit initial disturbance in the RWM mode amplitude.

Figure 12 shows the time response to initial conditions of the plasma, normalized to a starting RWM mode amplitude of 1 G. This simulation is performed at

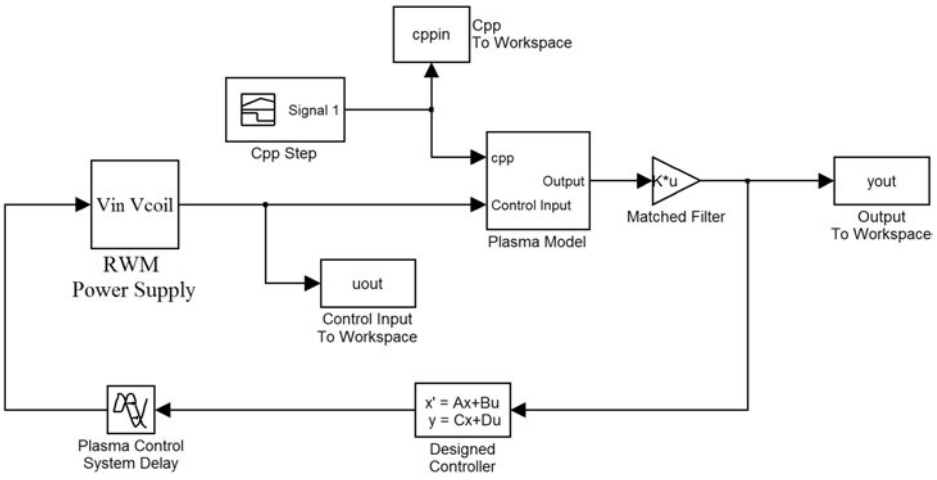

Fig. 10. Top level of the Simulink model.

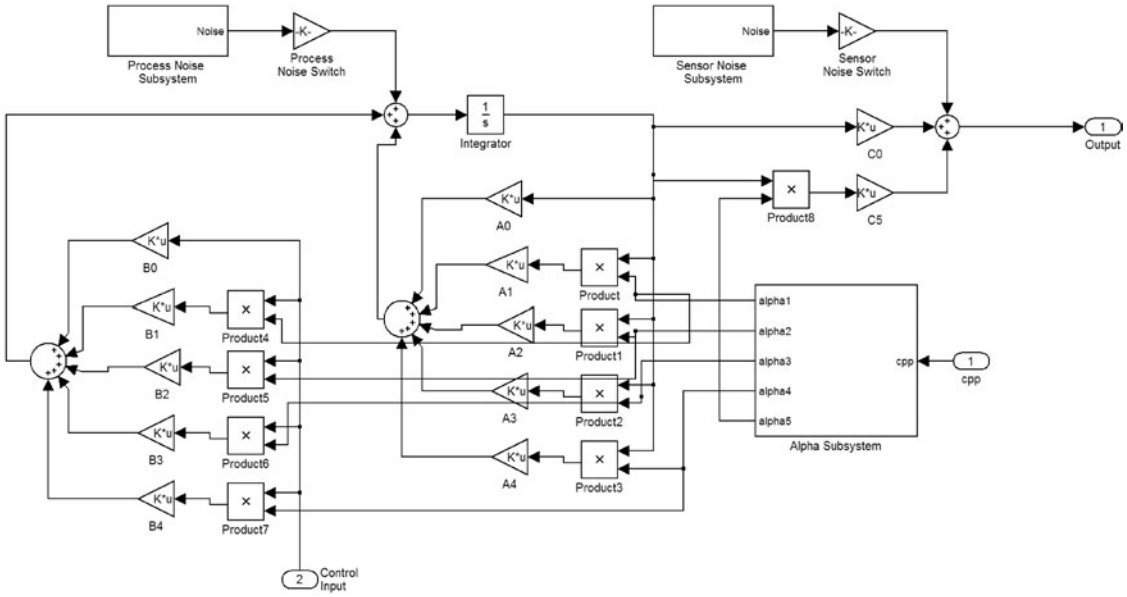

Fig. 11. Simulink model of the parameterized plasma state-space representation with noise.

constant RWM growth rates of $\gamma = 10$ rad/s and $\gamma = 5000$ rad/s, the lower and upper limits, respectively, of the growth rate range of our interest. In both cases, the *DK* controllers provide quick suppression of the RWM mode amplitude, outperforming the PD controller, which does not provide quick suppression at the faster growth rate (failing the performance criteria) and even shows a longer settling time for the slower growth rate when compared to the *DK* controllers. The applied coil voltages are shown in Figs. 13, 14, and 15 for the three cases. The three curves in Figs. 13, 14, and 15 are the three independent input control voltages to the I-coils in the quartet configuration. For both growth rates, the weighted *DK* controller design uses less applied voltage to achieve similar results. It is possible to note from Fig. 15, particularly from Fig. 15b (faster growth rate), that the PD controller needs significantly larger coil voltages to stabilize the system, driving the actuators closer to saturation.

Another example is presented in Fig. 16, which shows the time response to a unit step disturbance in the RWM mode amplitude. Once again, this simulation is performed with constant growth rates, which define our range of interest. For the slower growth rate (Fig. 16a), the *DK* and PD controllers have similar time responses with ~20% overshoot, and a fast rise time. For the faster growth rate, the system remains stable for all the controllers, but the settling time is increased beyond the time range shown

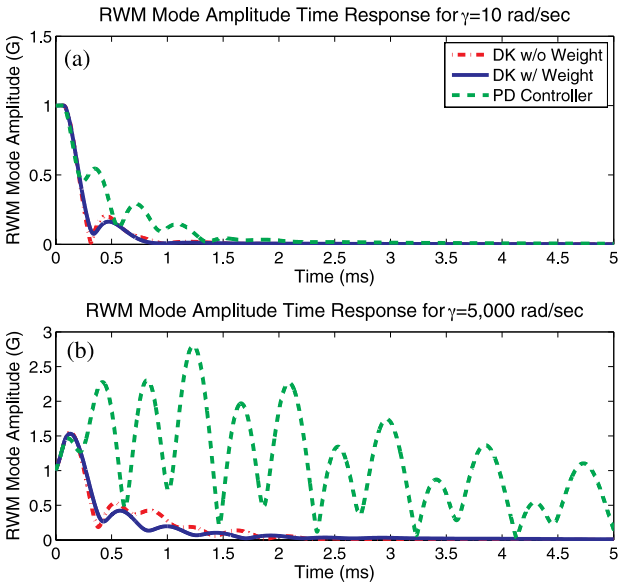

Fig. 12. Initial condition response RWM mode amplitude for (a) $\gamma = 10$ rad/s and (b) $\gamma = 5000$ rad/s with *DK* controllers.

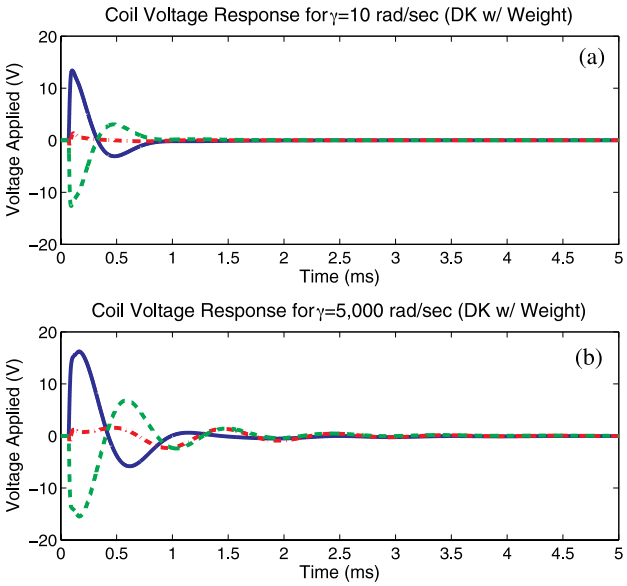

Fig. 14. Initial condition response control inputs for (a) $\gamma = 10$ rad/s and (b) $\gamma = 5000$ rad/s for *DK* with weight controller.

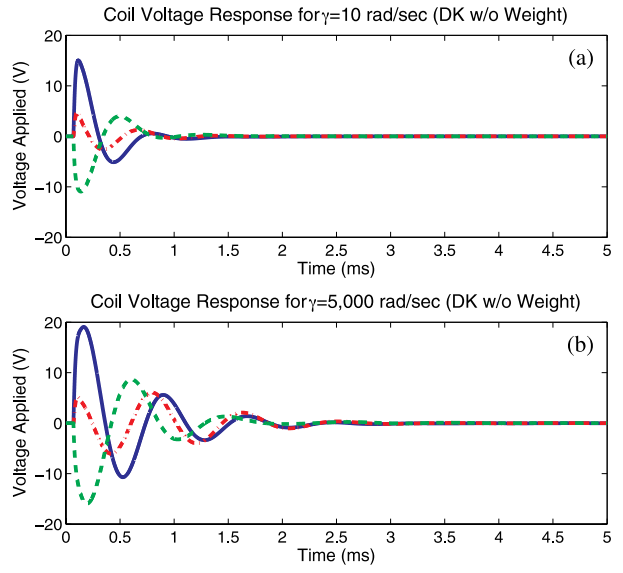

Fig. 13. Initial condition response control inputs for (a) $\gamma = 10$ rad/s and (b) $\gamma = 5000$ rad/s for *DK* without weight controller.

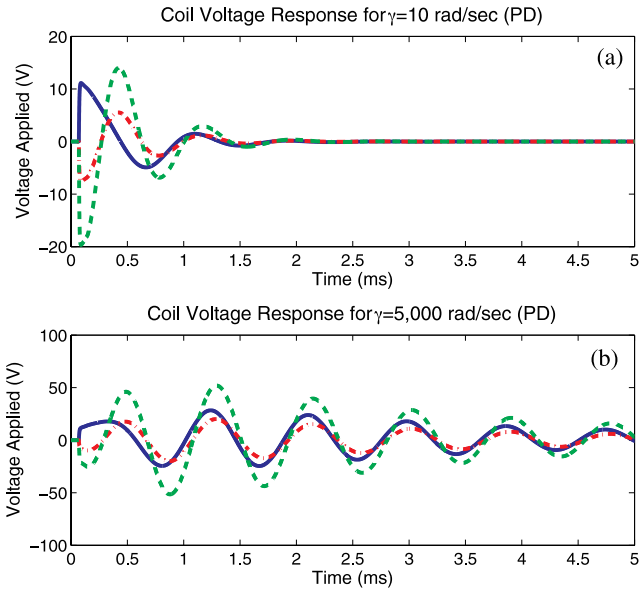

Fig. 15. Initial condition response control inputs for (a) $\gamma = 10$ rad/s and (b) $\gamma = 5000$ rad/s for PD controller.

in the figure. The PD controller, however, converges to a bigger steady-state offset when compared to the *DK* controllers.

IV.C. Closed-Loop Stability and Performance

It is useful to determine the range of γ where the system remains stable as well as the range where the system performs within the limits of the performance constraints (see Table I). Table II provides the ranges of γ for which stability and performance conditions are satisfied. The first row of Table II, "Stability range," indicates the range of γ for which the system remains stable when using a unit step disturbance input for the RWM model amplitude. The second row of Table II, "Performance range (initial)," indicates the range of γ

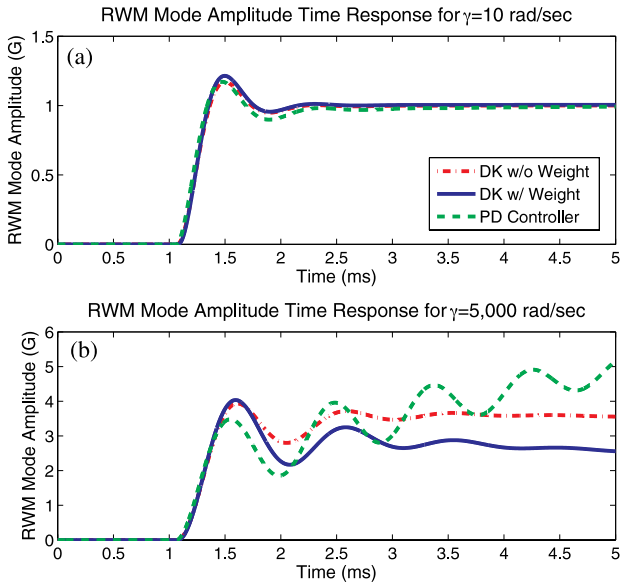

Fig. 16. Step response RWM mode amplitude for (a) $\gamma = 10$ rad/s and (b) $\gamma = 5000$ rad/s with *DK* controllers.

for which the performance conditions are satisfied when an initial unit excitation of the RWM mode amplitude is forced through appropriate initial conditions. Both model-based *DK* controllers show good stability and performance properties well beyond the desired γ range and that of the PD controller, with the weighted *DK* controller design having a larger range in both stability and performance.

As a final check of the controllers' performance, noise is added to the system to observe the predicted effect that it will have on the system. Only the sensor noise is taken into account, ignoring the process noise. The sensor noise is added to the set of 22 magnetic field sensors, before the matched filter is applied to the output. Tests are performed to find the root-mean-square (RMS) noise level of the RWM mode amplitude that can be sustained until instability is reached. The system is driven unstable in the presence of noise because of the saturation limits on the coil voltages. Table II summarizes the approximate RWM mode amplitude noise level at which this occurs. The Table II rows "RMS noise ($\gamma = 5000$ rad/s)" and "RMS noise ($\gamma = 2500$ rad/s)" correspond to initial condition response tests at growth rates of $\gamma = 5000$ rad/s and $\gamma = 2500$ rad/s, respectively. Both *DK* controllers can withstand larger amounts of sensor noise when compared to the PD controller. The PD controllers used in present experiments require substantial derivative gain for stabilization, which implies a large response to noise, leading to a requirement for high peak voltages and coil currents, which in turn lead to saturation and instability. It is important to recall at this point that as the growth rate increases, the PD controller works closer to saturation than the model-based *DK* controllers (see Fig. 15).

Since the robust controller stabilizes the plant over a range of growth rate, it is of interest to investigate the controller performance using a time-varying growth rate γ. The results for ramping, stepping, and sinusoidal excitation of the c_{pp} parameter are presented (Figs. 17, 18, and 19). The ramp function begins at an initial value of $\gamma = 120$ rad/s ($c_{pp} = 5.75$) and changes linearly to $c_{pp} = 0.3325$ over 5 ms. The step function also initiates at $c_{pp} = 5.75$ and changes between the maximum, nominal, and minimum values of c_{pp} in 0.5-ms intervals over a 2.5-ms span. The amplitude of the sinusoidal function is defined by the design range of c_{pp} used for the synthesis of the controller. Its frequency is 5000 rad/s. In all three cases, the RWM mode amplitude is quickly suppressed (Figs. 17, 18, and 19). Again, the weighted *DK* controller design maintains less RWM amplitude compared to the *DK* controller without weight, providing better rejection to changes in the growth rate. In all cases the PD controller has difficulty suppressing the RWM amplitude and becomes unstable in the stepping c_{pp} case.

V. CONCLUSIONS

The GA/FAR-TECH DIII-D RWM model was restructured into a robust control framework, isolating the RWM time-varying uncertain parameter c_{pp}, the key term influencing the size of the RWM instability. With the system model in this framework, the *DK*-iteration method was applied to develop robust controllers, as measured by the structured singular value, for a predetermined range of γ. Augmenting the nominal system

TABLE II

γ Stability and Performance Ranges

Controller	*DK* Without Weight	*DK* with Weight	PD
Stability range	0 to 7437 rad/s	0 to 8434 rad/s	0 to 5042 rad/s
Performance range (initial)	0 to 6459 rad/s	0 to 7150 rad/s	0 to 4103 rad/s
RMS noise ($\gamma = 5000$ rad/s)	15.12 G	12.03 G	1.16 G
RMS noise ($\gamma = 2500$ rad/s)	37.51 G	36.09 G	14.44 G

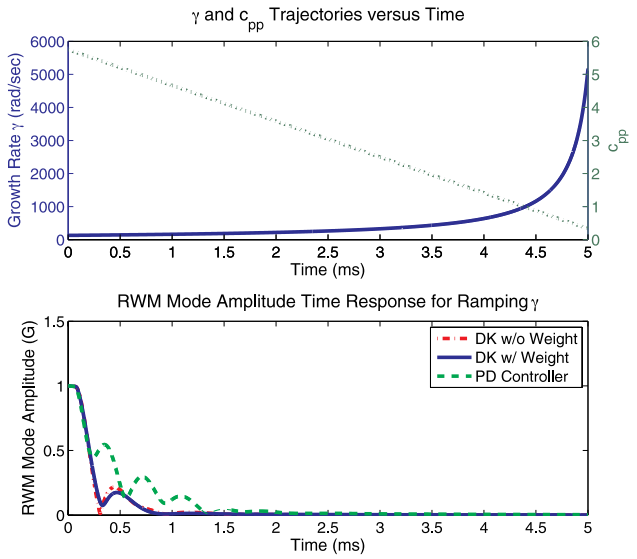

Fig. 17. Initial condition response control inputs for ramping γ with *DK* controller.

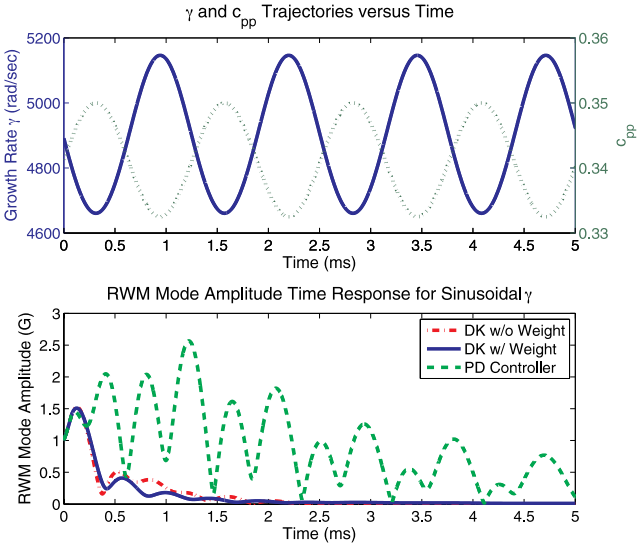

Fig. 19. Initial condition response control inputs for sinusoidal γ with *DK* controller.

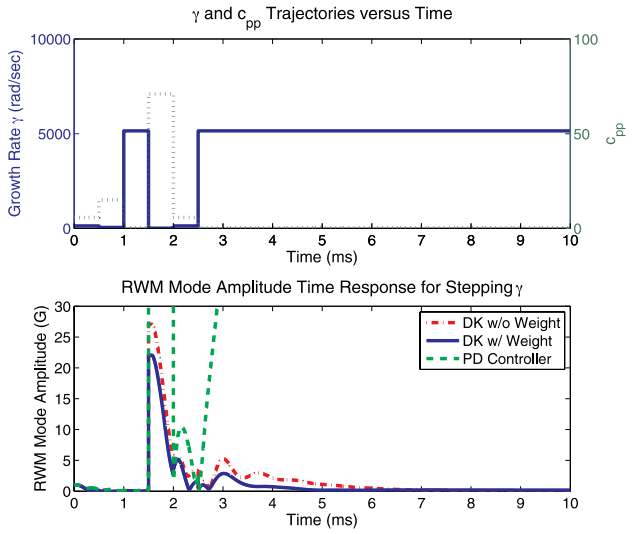

Fig. 18. Initial condition response control inputs for stepping γ with *DK* controller.

with performance weight provides better loop-shaping of the closed-loop system, which results in improved controller performance.

The *DK* controllers have been tested through simulations and compared with present PD controllers. The simulation study shows significant improvement over non-model-based PD controllers, increasing the RWM growth rate range for which the system is stable and satisfying predefined performance constraints. The simulation study also includes a comparison of the level of noise that can be withstood by the different controllers, showing that because of the derivative action the PD controller produces a larger response to noise, leading more easily to coil saturation and instability.

Since the plasma RWM growth rate can vary with operating conditions, the design of a controller that can stabilize the system over the entire physical range of γ is critical. The simulations show that the model-based *DK* controllers can successfully stabilize the mode for different types of time-varying growth rates. In terms of robust stability, this method eliminates the need of growth rate online identification and controller scheduling. Future work includes the experimental validation of this controller in DIII-D.

ACKNOWLEDGMENTS

This work was supported in part by a grant from the Commonwealth of Pennsylvania, Department of Community and Economic Development, through the Pennsylvania Infrastructure Technology Alliance, the National Science Foundation CAREER award program (ECCS-0645086), and the U.S. Department of Energy under contracts DE-FG02-92ER54141, DE-FC02-04ER54698, DE-FG02-03ER83657, and DE-FG03-99ER82791.

REFERENCES

1. M. L. WALKER et al., "Emerging Applications in Tokamak Plasma Control," *IEEE Control Sys. Mag.*, **26**, *2*, 35 (Apr. 2006).

2. A. PORTONE, F. VILLONE, Y. LIU, R. ALBANESE, and G. RUBINACCI, "Linearly Perturbed MHD Equilibria and 3D Eddy Current Coupling via the Control Surface Method Portone," *Plasma Phys. Control. Fusion*, **50**, *8*, 085004 (2008).

3. V. D. PUSTOVITOV, "General Formulation of the Resistive Wall Mode Coupling Equations," *Phys. Plasmas*, **15**, 072501 (2008).

4. Y. LIU, R. ALBANESE, A. PORTONE, G. RUBINACCI, and F. VILLONE, "An Analytical Demonstration of Coupling Schemes Between Magnetohydrodynamic Codes and Eddy Current Codes," *Phys. Plasmas*, **15**, 072516 (2008).

5. E. STRUMBERGER, P. MERKEL, M. SEMPF, and S. GUNTER, "On Fully Three-Dimensional Resistive Wall Mode and Feedback Stabilization Computations," *Phys. Plasmas*, **15**, 056110 (2008).

6. F. VILLONE, Y. Q. LIU, R. PACCAGNELLA, T. BOLZONELLA, and G. RUBINACCI, "Effects of Three-Dimensional Electromagnetic Structures on Resistive-Wall-Mode Stability of Reversed Field Pinches," *Phys. Rev. Lett.*, **100**, *25*, 255005 (2008).

7. C. M. FRANSSON, D. H. EDGELL, D. A. HUMPHREYS, and M. L. WALKER, "Model Validation, Dynamic Edge Localized Mode Discrimination, and High Confidence Resistive Wall Mode Control in DIII-D," *Phys. Plasmas*, **10**, *10*, 3961 (2003).

8. Y. IN et al., "Model-Based Dynamic Resistive Wall Mode Identification and Feedback Control in the DIII-D Tokamak," *Phys. Plasmas*, **13**, *6*, 062512 (2006).

9. H. REIMERDES et al., "Measurement of the Resistive-Wall-Mode Stability in a Rotating Plasma Using Active MHD Spectroscopy," *Phys. Rev. Lett.*, **93**, *13*, 135002 (2004).

10. S. A. SABBAGH et al., "Active Stabilization of the Resistive-Wall Mode in High-Beta, Low-Rotation Plasmas," *Phys. Rev. Lett.*, **97**, *4*, 045004 (2006).

11. D. H. EDGELL et al., "Magnetohydrodynamic Mode Identification from Magnetic Probe Signals Via a Matched Filter Method," *Rev. Sci. Instrum.*, **73**, *4*, 1761 (2002).

12. A. M. GAROFALO et al., "Resistive Wall Mode Dynamics and Active Feedback Control in DIII-D," *Nucl. Fusion*, **41**, *9*, 1171 (2001).

13. M. OKABAYASHI et al., "Active Feedback Stabilization of the Resistive Wall Mode on the DIII-D Device," *Phys. Plasmas*, **8**, *5 II*, 2071 (2001).

14. E. J. STRAIT et al., "Resistive Wall Mode Stabilization with Internal Feedback Coils in DIII-D," *Phys. Plasmas*, **11**, *5 II*, 2505 (2004).

15. M. OKABAYASHI et al., "Control of the Resistive Wall Mode with Internal Coils in the DIII-D Tokamak," *Nucl. Fusion*, **45**, *12*, 1715 (2005).

16. S. MAUEL et al., "Dynamics and Control of Resistive Wall Modes with Magnetic Feedback Control Coils: Experiment and Theory," *Nucl. Fusion*, **45**, *4*, 285 (2005).

17. S. SABBAGH et al., "The Resistive Wall Mode and Feedback Control Physics Design in NSTX," *Nucl. Fusion*, **44**, *4*, 560 (2004).

18. J. R. DRAKE et al., "Experimental and Theoretical Studies of Active Control of Resistive Wall Mode Growth in the EXTRAP T2R Reversed-Field Pinch," *Nucl. Fusion*, **45**, *7*, 557 (2005).

19. D. YADIKIN, P. R. BRUNSELL, and J. R. DRAKE, "Intelligent Shell Feedback Control in EXTRAP T2R Reversed Field Pinch with Partial Coverage of the Toroidal Surface by a Discrete Active Coil Array," *Plasma Phys. Control. Fusion*, **48**, *1*, 1 (2006).

20. D. YADIKIN, P. R. BRUNSELL, and R. PACCAGNELLA, "Advanced Feedback Control Methods in EXTRAP T2R Reversed Field Pinch," *Phys. Plasmas*, **13**, *7*, 72109 (2006).

21. P. R. BRUNSELL, K. E. J. OLOFSSON, L. FRASSINETTI, and J. R. DRAKE, "Resistive Wall Mode Feedback Control in EXTRAP T2R with Improved Steady-State Error and Transient Response," *Phys. Plasmas*, **14**, *10*, 102505 (2007).

22. S. ORTOLANI, "Active MHD Control Experiments in RFX-mod," *Plasma Phys. Control. Fusion*, **48**, *12B*, B371 (2006).

23. R. PACCAGNELLA, D. TERRANOVA, and P. ZANCA, "Modelling and Interpretation of MHD Active Control Experiments in RFX-mod," *Nucl. Fusion*, **47**, *8*, 990 (2007).

24. A. SOPPELSA, G. MARCHIORI, L. MARRELLI, and P. ZANCA, "Design of a New Controller of MHD Modes in RFX-mod," *Fusion Eng. Des.*, **83**, *2–3*, 224 (2008).

25. A. K. SEN et al., "Optimal Control of Tokamak Resistive Wall Modes in the Presence of Noise," *Phys. Plasmas*, **10**, *11*, 4350 (2003).

26. Z. SUN et al., "Adaptive Optimal Stochastic State Feedback Control of Resistive Wall Modes in Tokamaks," *Phys. Plasmas*, **13**, *1*, 012512 (2006).

27. O. KATSURO-HOPKINS et al., "Enhanced ITER Resistive Wall Mode Feedback Performance Using Optimal Control Techniques," *Nucl. Fusion*, **47**, *9*, 1157 (2007).

28. K. ZHOU, J. C. DOYLE, and K. GLOVER, *Robust and Optimal Control*, Prentice Hall, Englewood Cliffs, New Jersey (1996).

29. A. H. BOOZER, "Error Field Amplification and Rotation Damping in Tokamak Plasmas," *Phys. Rev. Lett.*, **86**, *22*, 5059 (2001).

30. T. KAILATH, *Linear Systems*, Prentice Hall, Englewood Cliffs, New Jersey (1979).

31. A. K. PACKARD, "What's New with μ: Structured Uncertainty in Multivariable Control," PhD Thesis, University of California, Berkeley (1988).

32. S. SKOGESTAD and I. POSTLETHWAITE, *Multivariable Feedback Control; Analysis and Design*, Wiley, New York (2005).

33. P. M. YOUNG, "Controller Design with Real Parametric Uncertainty," Technical Memorandum CIT-CDS 93-016, California Institute of Technology (1993).